Analytic Solutions for Fresh Groundwater Lenses Floating on Saline Water Under Desert Dunes: the Kunin-van der Veer Legacy Revisited

A.R.Kacimov[1], *Yu.V.Obnosov*[2]

[1]Department of Soils, Water and Agricultural Engineering, Sultan Qaboos University, Oman
anvar@squ.edu.om, akacimov@gmail.com
ORCID ID: orcid.org/0000-0003-2543-3219

[2]Institute of Mathematics and Mechanics, Kazan Federal University, Kazan, Russia
yobnosov@kpfu.ru
ORCID: orcid.org/0000-0001-9220-7989

Technical Note

Short title for running head: Floating fresh water lenses

Submitted to J. of Hydrology (Elsevier)

On September 10, 2018 as manuscript HYDROL29272
first set of referees comments received on December 12, 2018;
first revised version submitted: on January 18, 2019;
second set of referees comments received on …;
second revised version submitted: on … ;
accepted:.... rejected: .....

Address for correspondence:
Prof. Kacimov A.R., Department of Soils, Water and Agricultural Engineering
Sultan Qaboos University Al-Khod 123, PO Box 34 Sultanate of Oman
Tel (968) 24141-201 Fax (968) 24413-418
Emails: anvar@squ.edu.om
akacimov@gmail.com
Omani page:
https://www.squ.edu.om/agr/Academics/Departments/Soil-Water-and-Agricultural-Engineering

Analytic Solutions for Fresh Groundwater Lenses Floating on Saline Water Under Desert Dunes: the Kunin-van der Veer Legacy Revisited

A.R.Kacimov, Yu.V.Obnosov

Abstract. A fully-saturated lens of steady fresh groundwater floating in a homogeneous and isotropic desert sandy aquifer is analytically studied based on a hydrological model by Kunin and interface solution by Van Der Veer. A static saline groundwater is beneath the lens. A phreatic surface of moving fresh water inside the lens is partially recharged (either naturally or by managed aquifer recharge) from the vadose zone and partially exfiltrates to it. A spatially focused recharge and intensive evapotranspiration preserve a steady downward-upward topology of fresh water motion. In terms of the 1-D Dupuit-Forchheimer approximation in a horizontal in-lens saturated flow a boundary value problem (BVP) for an ODE for the Strack potential is solved. The shape of the water table and, based on the Ghijben-Herzberg assumption , the interface are found. The total volume of the positive-pore pressure water flowing within the lens is evaluated. Constant infiltration and evaporation rates as well as evaporation linearly decreasing with depth of the water table (counted from the ground surface) are considered. The case of 2-D flow is tackled by the Toth model. A triangular analytic element approximates a half of the flow domain and consists of an isobaric side and two no-flow sides. Conformal mapping of this triangle onto a reference plane and solution of the Dirichlet BVP in a half-plane deliver the distribution of infiltration-exfiltration intensity along the water table, total flow rate and locus of the hinge point. A mathematically more cumbersome approximation of the flow domain assumes the water table to be a tilted straight line but the interface to be found as a free boundary. Solution of the corresponding BVP uses a curvilinear triangle in the hodograph plane.

Key words: fresh-saline groundwater, interface, phreatic surface, conformal mappings,

2-D Tothian and 1-D Dupuit-Forchheimer flow models, hydrology of arid desert dunes.

"When you're in the muck you can only see muck. If you somehow manage to float above it, you still see the muck but you see it from a different perspective. And you see other things too. That's the consolation of philosophy."

David Cronenberg

1. Introduction

Fresh groundwater lenses are formed in coastal aquifers, oceanic islands and wetlands due to rainfall-induced recharge to the lens phreatic surface (see e.g. Chesnaux and Allen, 2008, Eeman et al., 2011, Houben et al. , 2014a, Houben et al., 2014b, Houben et al., 2018, Schot et al., 2004, Vacher, 1988, van der Veer, 1977, Werner and Laattoe, 2016). Fresh-saline interface is a part of the boundary of such lenses, found and investigated in Bermuda, Germany, Holland, Paraguay, and other countries. The interface crops out into a well-defined surface water body (sea, river, lake or drainage ditch) into which a light fresh groundwater discharges.

Terrestrial freshwater lenses (TFLs) in arid or semi-arid climates are not in a direct and permanent contact with surface water (see Fig.2a, d in Laattoe et al., 2017). Fresh floating groundwater lenses (hereafter abbreviated as FFGLs) are a special type of TFLs. FFGLs are subtended by an interface and capped by a phreatic surface recharged from the vadose zone. Post-rain infiltration or ephemeral ponding of topographic depressions filled after occasional runoff is balanced by evaporation from the phreatic surface, if it is shallow enough. For example, Hampton (1963) for lenses in Oregon estimated evaporation from the phreatic surface of lenses in coastal dunes as 7 inches/year and pointed out: "*In parts of the area where the water table is shallow and the vegetation is dense, the evapotranspiration doubtless is much greater;*

conversely, in the barren dune areas, and at places where the water table is relatively deep, the evapotranspiration probably is considerably less than 7 inches per year." Emikh (1963) analytically studied channel-fed TFLs in Central Asia (see the corresponding sketch in Fig.2b of Laattoe et al. 2017) for which evaporation was assumed the only factor discharging groundwater from the lens.

FFGLs have been detected and studied in Australia, Kuwait, Nambia, Oman, UAE (see e.g. Al-Weshah and Yihdego, 2016, Cendón et al., 2010, Kwarteng et al., 2000, Laattoe et al., 2017, Macumber, 2003, Milewski et al., 2014, Rizk and Al-Sharhan, 2003, Young et al., 2004). Unlike humid lenses in Europe (Voortman et al., 2015), infiltration-evaporation on the water table of these FFGLs and ensued groundwater motion inside is much less investigated (Laattoe et al., 2017).

In this paper, we use the studies of Kunin (1959)[1] in the Karakum desert of Turkmenistan. A large-scale water supply from FFGLs in Central Aisa started in the 1960s, with the arrive of the Soviet oil-gas industry to the deserts of this region that required much more fresh water than the local traditional animal husbandry. Bairamova (2013) reports that pumping from one of the largest TFLs in Turkmenistan commenced in 1963, with 56 well galleries drilled in 1963-1969; 49 of them are being exploited around 40 years. A common interface delineating TFLs is a 1g/l isoconcentric surface. Bairamova (2013) emphasizes that the genesis of TFLs (including FFGLs) in Turkmenistan is still not well understood.

Pumping from TFLs of these deserts was compounded with managed aquifer recharge (MAR) through engineered infiltration ponds placed just above the lenses (see the photos of the Sansyz MAR project, retrieved from Kunin, 1959, supplementary file 1). These excavations harnessed the natural occasional runoff and converted it into an intensive infiltration spot

[1] Dr. Vladimir Kunin (1906-1976), the corresponding member of the Academy of Sciences of USSR, one of the founders of the Institute of Deserts (city of Ashkhabad), Turkmen Academy of Sciences of the Turkmen Soviet Socialist Republic, published extensively on hydrology of deserts (see e.g. Kunin, 1968).

(analogous to ones shown in Fig.2 of Stuyfzand and van der Schans, 2018 for similar lenses in Holland). Without such simply engineered rainwater collectors the desert runoff is either lost to draining channels or gets diffused as a low-intensity infiltration to those parts of the desert, where the sand moisture redistributes to evaporation i.e. stable FFGLs can not be formed. Kunin (1959) and Schevchenko (1965), depending on topography and desert soil cover, distinguished three types of desert TFLs, *viz.* small sub-dune FFGLs (Fig.1a), small FFGLs under topographic depressions, called takyrs (Fig.1b) and megalenses. Natural hydraulic gradients of several unconfined aquifers (salinity of chloride-type saline groundwater is 20-40 g/l), common in Turkmenistan (Kunin, 1959, Rogovskaya et al., 1986), are adverse to retaining FFGLs even if infiltration is sufficient and spatially focused. Unlike under hydrological conditions of Holland, FFGLs in Turkmenistan can not be replenished by diversion of surface fresh water from perennial streams because they do not exist in the desert.

If a bedrock in Fig.1 is not deep enough (see also Danin, 2012, Fig.78) and the pristine unconfined saline groundwater is not thick enough, then a lens is not FFGL. In Fig.1b the corresponding lens is demarcated by the contour $E_1E_2E_3E_4E_1$. A horizontal segment of the bedrock, E_4E_1, subtends this lens. It can be stable even without evaporation from the phreatic surface E_2E_3, provided fresh groundwater seeps through a slightly permeable line E_4E_1, as in Kacimov and Obnosov (2015). A deep borehole drilled across FFGL would show the following zonation: vadose zone –fresh water table – fresh groundwater zone - interface between fresh and saline water - saline groundwater -deep bedrock.

The topographic depressions (natural ones or engineered excavations) of an appropriate locale, sizes and placed above right phreatic saline phreatic surfaces convert a runoff of sufficiently strong rain into FFGLs which can be diligently abstracted (Kunin and Leszhinsky, 1960). As a prerequisite of existence of FFGL, Rogovskaya et al. (1979) pointed out that too small thicknesses of the vadose zone above the lens "*lead to dissipation of the ground water by plant uptake, with some substantial salt accumulation*" and "*an aeration zone of*

thickness less than 3 m in conjunction with lack of plant cover results in highly saline water due to physical evaporation."

Intelligent MAR operations in replenishing the exploited FFGLs of Turkmenistan, in addition to natural recharge, incorporated skimming of fresh water by vertical wells, collated with a simultaneous pumping of a subjacent saline water of FFGLs. This pioneering dual-pumping controlled the fresh-saline water interface. Such mitigation of upconing of saline water in FFGLs and ensuring their resilience commenced in 1963, prior to many similar projects in the USA or Holland (see e.g. Singh and Stammers, 1989, Zuurbier et al., 2014).

The very existence of a stable FFGL is conditioned by the following factors:

- There should be saline/brine background water table on which the lenses emerge as hydrogeological buoys that is illustrated in Fig.1 a-f of Laattoe et al., 2017;
- The natural gradient of this subjacent background saline groundwater should be small, i.e. away from the lens the water table should be almost flat because otherwise FFGL slips downgradient (Kunin, 1959) and/or gets dispersed by the subjacent saline groundwater;
- The thickness of the vadose zone above the phreatic surface of the lens should be appropriate. Otherwise, infiltration and evaporation do not make a favourable source-sink hydrodynamic couple similar to one in Kacimov et al. (2018). Juxtaposition of recharge to the water table and losses from it maintains a continuous motion of fresh water within the lens.
- Transpiration intensity by natural hydromorphic plants (if any) on the ground surface above the lens should be bounded both from above and below. No transpiration may result in high water table and its salinization. Too intensive interception of groundwater by the roots may eventually deplete the lens and, consequently, exterminates the plants.

Natural recharge and MAR to and pumping from FFGLs for drinking (both by humans and livestock) are going on in modern Turkmenistan (Babaev, 1999). A post-Kunin review of hydrology, hydrogeology, climate, topography, geomorphology, soil cover and water consumption in deserts of Turkmenistan is reported by Babaev (1999), Bairamova (2013), Fleskens et al. (2007), Hydrogeology…(1972), Kolodin (1981).

Typical concentrations of total dissolved solids (TDS) of fresh and saline groundwater in FFGLs are about 1 g/l and 20-60 g/l (respectively). Kunin (1959) modeled a thin transition zone by a Ghijben-Herzberg interface. The field data on the vertical profile of TDS in the Sansyz FFGL is shown in supplementary file 2 (retrieved from Kunin, 1959). This cross-section illustrates that close to point C in our Fig.1a the thickness of the transition zone between isoconcentric contours 1 g/l and 10 g/l is about 1-2 meters (the maximal thickness of the lens is about 12 m). Towards point A in our Fig.1a the Kunin interface is blurred i.e. the distance between isolines of 1 g/l and 10 g/l becomes large.

The thickness of small FFGLs can be several tens of centimeters only. These mini-lenses are tapped by dug wells and fresh water is occasionally and carefully consumed by local nomads. The bed of takyrs gets gradually clogged due to mechanical colmatation (see the photos of a dry takyr retrieved from Kunin, 1959, supplementary file 3).

In a vertical cross-section of FFGL (Fig.1a) the dune is symmetric with respect to a vertical axis O*Y* of Cartesian (*XOY*) or cylindrical (*ROY*) coordinate systems. A horizontal axis is O*X* or O*R*, respectively. This axis coincides with the background level of saline groundwater. If no infiltration and no fresh water present, the saline water table is a plane. The curve $B_sM_sC_s$ in Fig.1a is the ground surface contour. Due to symmetry, below only the right half of the dune is considered. FFGL is bounded from above by a phreatic surface *BMC* and from below by an interface *AC*. The separatrix *BOC* in Fig.1a is a vertical segment.

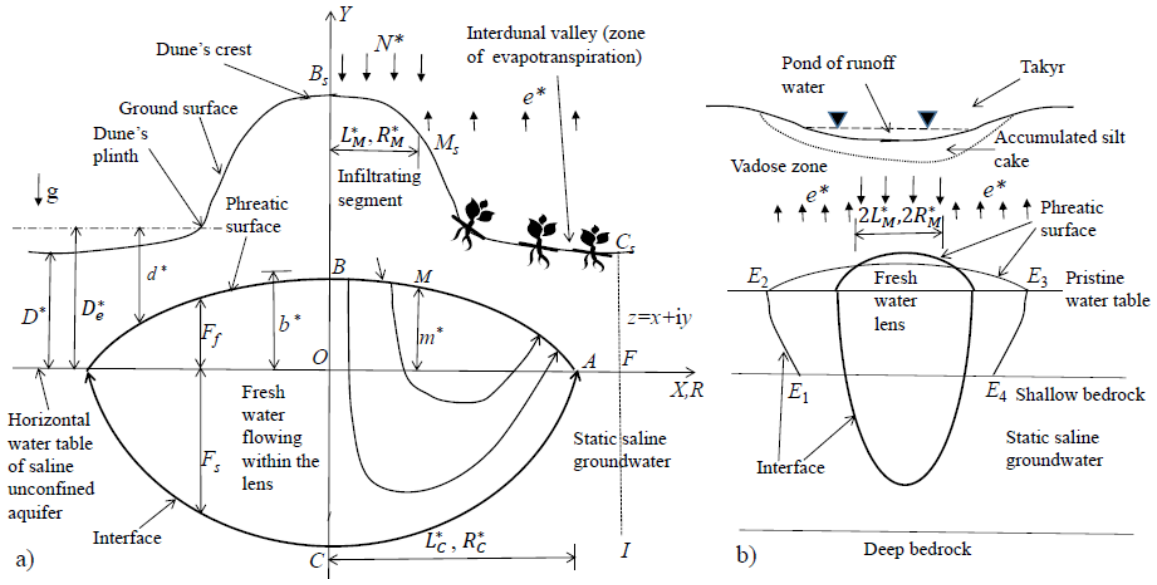

177

178 Fig.1 Vertical cross-section of FFGL recharged from a linear dune (a) and from a takyr (b).

179 The following questions intrigued arid zone hydrologists in Turkmenistan: why does a stable
180 FFGL in Fig.1a exist and why is it digon-shaped? Why the curve *BMA* is a subdued replica of
181 B_sC_s (the topography of the dune) and *AC* is an amplified, Ghijben -Herzbergian replica of *BMA*?
182 In other words, can one extend the criterion of Haitjema and Mitchell-Bruker (2005, their
183 eqn.(8)) of topography-recharge controlled phreatic surface flows to *BMA* in Fig.1a, which has
184 a focused infiltration strip (disk) under a dune (or ponded takyr bed)?

185 Unlike the situations of common deep or shallow unconfined aquifers in Haitjema and
186 Mitchell-Bruker (2005) and their assumption of a constant accretion on the water table, FFGLs
187 in our Fig.1 have a large variation of its fresh water thickness, F_s+F_f. Flow in our Fig.1 is a
188 conjugation of flows in Figs.1 and 8 of Van Der Veer (1977), i.e. a source-sink boundary
189 condition along a phreatic surface (recharge under the crest of the dune and evaporation on the
190 flanks) makes the situation different form one in Haitjema and Mitchell-Bruker (2005). The
191 groundwater systems modeled by Haitjema and Mitchell-Bruker (2005) and Toth (2009) are
192 common for humid climates where evaporation from the phreatic surface is not a major factor. In
193 our case, the evaporation rate, e^*, from segment *AM* of the phreatic surface in Fig.1a is high and
194 may depend on d^*, the depth of the phreatic surface under an average terrain surface.

In this paper, we propose a plausible explanation of the existence of FFGLs: a stable lens is a result of a spatial alteration (with the X or R coordinate in Fig.1a) of the boundary condition along the water table. Namely, infiltration occurs from the crest zone, B_sM_s, of a fixed width and evapotranspiration takes place from the plinth-valley zone, M_sC_s the width of which is a part of solution. We emphasize that – similarly to Emikh (1963) - the lens in Fig.1a is much wider than the hill and zone of infiltration from above, B_sM_s. This is different from oceanic lenses the shape of which is determined by the topographic hill shape. In desert TFLs, the width of the lens is controlled by evapotranspiration which dominates in a relatively flat zone M_sC_s of Fig.1a.

The near-surface sand at the crest of tall desert dunes is coarser and more permeable than that at the slopes and interdunal depressions. The crests are commonly not covered by biocrust, vegetation or fine sediment, while the lower slopes and interdunal valleys are (e.g. Chamizo et al., 2016, Kidron and Yair, 2008, Fig. 17.2, Pye and Tsoar, 2008, Fig.7.28, 9.6; Yair et al, 2008, Figs.2.2,24). The infiltration rate on the crest is higher than along the dune slopes and in the valley (see e.g. Lopez, et al., 2015, Tao et al., 2001), provided the sand is not hydrophobic. Annual evaluations of N^* in loose sands give values which are several times higher than in vegetated, silt-clay clogged and biocrusted sands (see e.g. Gael and Smirnova, 1999). In humid climates, however, the dune crests can be covered by moss (see e.g. Voortman, 2018) and the water-repellent sand makes the infiltration distribution to subjacent fresh groundwater lenses more complex: less recharge comes through a zone on the dune crest as compared with the slopes and valley (see e.g. Houben, et al., 2014a).

In satellite images or aerial views, the green cover depicted in Fig.1a, makes a distinct spatial pattern of ecotones monitored also by botanists on the ground (see e.g. Dedkov, 2011). For example, the black *saksaol* trees on the slopes and interdunal areas of the Repeteka National Park in Turkmenistan strongly depend on the subsurface hydrology. As these plants grow, transpiration increases and climatic conditions (i.e. recharge through the curve *BM* and

distributed losses to the vadose zone along *MC* in Fig.1a) remain stable. The lens starts to shrink because of a more intensive subsurface water uptake by *saksaol* roots that results in degradation of the trees. That biome-lens dynamics is in comport with what Toth (2009) reported in his Section 4.4.2.3. Devegetation also impacts the hydraulic and capillary properties of the vadose zone (see e.g. Wang et al., 2015).

It is noteworthy that dunes in our Fig.1a are sufficiently tall. For less-bulging desert landforms, *viz.* small-size sand piles, the hillocks (the so-called nebkhas), plants grow on the crest of the hillocks, see e.g. Danin (2012, Figs. 16, 21, 51, 62), Khalaf et al. (1995).

On an annual and decadal time-scale, the segment *BM* of the phreatic surface in Fig.1a is grossly a zone of recharge of FFGL of lateral extension L_M^* or R_M^* (2-D and axisymmetric cases, respectively). The segment *MC* of horizontal sizes L_C^* or R_C^* is a zone of a distributed exfiltration (evapotranspiration) from the lens. Correspondingly, the recharge-discharge distribution along the phreatic surface in Fig.1a is exactly the same as in Strack (1978), who considered an unconfined aquifer (without a subjacent interface and bedrock deep at infinity). Van Der Veer (1977) studied a semi-infinite wedge of a fresh water commingled with a static sea water intrusion tongue. We combine the analytic components of Strack's and Van Der Veer 's flow models: the curve *BMA* caps FFGL in Fig.1a and *AC* reflects its confining and floatational features. We note that transient variable-density flows in the takyr MAR-fed FFGLs of Turkmenistan have been numerically modeled by FEFLOW (Kuznetsov et al., 2006, Yakirevich et al., 2005).

Dynamics of fresh groundwater in Fig.1a is similar to what has been studied in the Toth (2009) regional flow model, in which a rigid bedrock commonly serves as a confining boundary of fresh groundwater flows (see e.g. his Figs. 2.1, 2.2, 3.1,3.2, 3.6-3.14, 3.22, 4.1, 4.16, 5.26, 5.34-5.38, 5.51, 5.67). The Toth-type topology of streamlines shown in Fig.1a is corroborated by Yair (2008): "*The long-term effect of subsurface lateral water flow is supported by data on*

246 *changes in electrical conductivity and amount of fine-grained material at the base of the dune*
247 *slopes. Wedges of increased salinity and content of fine-grained particles, parallel to the sloping*
248 *surfaces, were detected at the slope bases (Fig.* 18.11*).*" Yair experimentally proved that near
249 point B_s (recharge zone) in our Fig.1a soil water inside the dune is an order of magnitude less
250 saline than near the dune pedestal (evaporation zone). Obviously, for artificially recharged
251 FFGL depicted in Fig.1b (see also Kunin and Lezshinsky, 1960) the schematization of Fig.1a
252 is adopted to a takyr topography, *viz.* a zone of engineeringly controlled L_M^* or R_M^* specified by
253 the size of a infiltration basin (natural or constructed). The basin can be linear, circular or of a
254 more complex shaped (Yakirevich et al., 2005, Kuznetsov et al., 2006). In Fig.1b, instead of an
255 elevated highly permeable dune crest above FFGL of Fig1a, a low permeable and depressed
256 colmatation layer feeds the lens.

257 One of the motives in studying FFGL in Fig.1 stems from the necessity to prepare for a
258 possible water shortage and corresponding planning for the extraction of water resources in the
259 deserts. As Porter (2015) pointed out, the whole world is not flat i.e. in our application to
260 topography in Fig.1a, FFGLs stored under undulating sandy ground surface may become a
261 vital reservoir for the desert settlements when regular aquifers are depleted or contaminated .

262 **2. Conceptual Model**

263 We assume a steady-state, Darcian, capillarity-free (one-phase, fully saturated) 2-D flow in
264 FFGL formed in a sand of hydraulic conductivity *k*. A light pore water of density ρ_f floats on a
265 static dense saline water of density ρ_s with an interface *AC*. Dispersion is ignored.

266 FFGL in Fig.1a is recharged by infiltration of intensity $N^*(X)>0$ which arrives at a segment
267 *BM* of a given length L_M^* of the phreatic surface from a zone B_sM_s of the dune crest, similarly to
268 the case of infinite strip islands (Chesnaux and Allen, 2008, Vacher, 1988). The evaporation
269 of intensity $e^*(X) >0$ – unlike the island lenses - takes place from *MA*. The ordinate of point *A* is

apriori unknown. Fresh groundwater evaporates from FFGL and from a horizontal segment AF of a static saline water table. On the ground surface, the corresponding curve M_sC_s extends to the point C_s, the middle of the interdunal valley. The ray C_sFI in Fig.1a separates the modeled dune from its neighbor on the right. Measurements or even assessments of e^* are more problematic than of N^* (see e.g. Hampton, 1963).

We consider a solitary lens i.e. we assume that N^* is small enough and e^* is high enough such that L_C^* is narrow enough i.e. the lenses under two neighbouring dunes do not interfere. If $N^*=e^*=0$, then the water table of the ambient static saline groundwater coincides with the axis Ox.

The streamlines in Fig.1a, bounded by a separatrix *BOC*, illustrate the Toth-type flow of fresh groundwater within the lens, with a hinge point *M* (point on the phreatic surface where infiltration changes to exfiltration). The position of the phreatic surface of the lens $F_f(X)$, in particular, the elevations b^* and m^* of the points *B* and *M*, the horizontal size of the lens L_C^* (the ordinate of the point *C* where the phreatic surface and interface intersect) and the locus of the interface $F_s(X)$ are to be found.

3. Dupuit-Forchheimer Approximation

3.1 Planar flow

In the Dupuit-Forchheimer (DF) model (see e.g. Bakker, 2000, Eeman, 2017, Polubarinova-Kochina, 1977, Strack, 1989, Van Der Veer, 1977, Van Duijn and Schotting, 2017), steady 1-D flow in FFGL obeys the ODE:

$$\frac{\mathrm{d}}{\mathrm{d}X}\left(k\,(F_f+F_s)\frac{\mathrm{d}F_f}{\mathrm{d}X}\right)=\begin{cases}-N^*(X), & \text{at} \quad 0\le X\le L_M^*,\\ e^*(X), & \text{at} \quad L_M^*\le X\le L_C^*.\end{cases} \tag{1}$$

where F_s is the interface ordinate, which is related to the phreatic surface as

$$F_s=F_f/\gamma,\gamma=(\rho_s-\rho_f)/\rho_s. \tag{2}$$

For water supply schemes and MAR, the volume, Ar^*, of fresh water stored in FFGL is of primary interest.

We introduce dimensionless quantities:

$$(g_s, g_f, x, y, b, m, L_C) = (F_s, F_f, X, Y, b^*, m^*, L_C^*) / L_M,$$

$$Ar = Ar^* / L_M^2, \quad (N, e) = (N^*, e^*) / (k(1+1/\gamma)).$$

which represent the geometric and hydrological characteristics of FFGL.

Then, using eqn.(2) the governing eqn.(1) is written:

$$\frac{\mathrm{d}^2 \Phi_f}{\mathrm{d}x^2} = \begin{cases} -N(x), \text{ at} & 0 \le x \le 1, \\ e(x), \quad \text{at} & 1 \le x \le L_C, \end{cases} \tag{3}$$

where $\Phi_f = g_f^2 / 2$ is Strack's (1989) potential, and $Q(x) = -\mathrm{d}\Phi_f / \mathrm{d}x$ is the vertically integrated dimensionless discharge. At x=0 and $x=L_c$ the discharge Q=0. Three other boundary conditions for solving eqn.(3) are: $Q(x)$ and $\Phi_f(x)$ are continuous functions at the hinge point M (x=1). We note that $N(1) \neq e(1)$ i.e. the sink-source intensity in the RHS of eqns.(1),(3) is discontinuous. Also in Fig.1a the lens tapers to point A i.e. $\Phi_f(L_C) = 0$.

From annual hydrological balances of precipitation-evapotranspiration we assume that $N=N_0$=const > 0, $e=e_0$=const > 0. Then, similarly to Kacimov et al. (2009), after simple algebra solution to the BVP (3) with the above stated boundary conditions is:

$$g_f = \begin{cases} \sqrt{N_0(1+N_0/e_0) - N_0 x^2}, \text{ at} & 0 \le x \le 1, \\ \sqrt{e_0}(1+N_0/e_0 - x), \quad \text{at} & 1 \le x \le L_C = 1 + N_0/e_0, \end{cases} \tag{4}$$

Obviously, from eqn. (4) the infiltrating branch *BM* of the phreatic surface is an arc of an ellipse with its summit at point *B* where $b = \sqrt{N_0(1+N_0/e_0)}$ and the evaporating branch *MC* is a straight tilted line (as was the evaporating phreatic surface of Van Der Veer, 1977, his Fig.8). Clearly, according to the Ghijben-Herzberg approximation $g_s=g_f/\gamma$.

A dimensionless cross sectional area, *Ar*, of the curvilinear triangle *ABCA* is:

$$Ar = (1+1/\gamma)\int_0^{1+N_0/e_0} g_f(x)\,\mathrm{d}x = (1+1/\gamma)\left(\frac{N_0}{2\sqrt{e_0}}\left(1+\frac{N_0}{e_0}\right)+\frac{\sqrt{N_0}}{2}\left(\frac{N_0}{e_0}+\left(1+\frac{N_0}{e_0}\right)\arctan\left[\frac{1}{\sqrt{e_0}}\right]\right)\right), \quad (5)$$

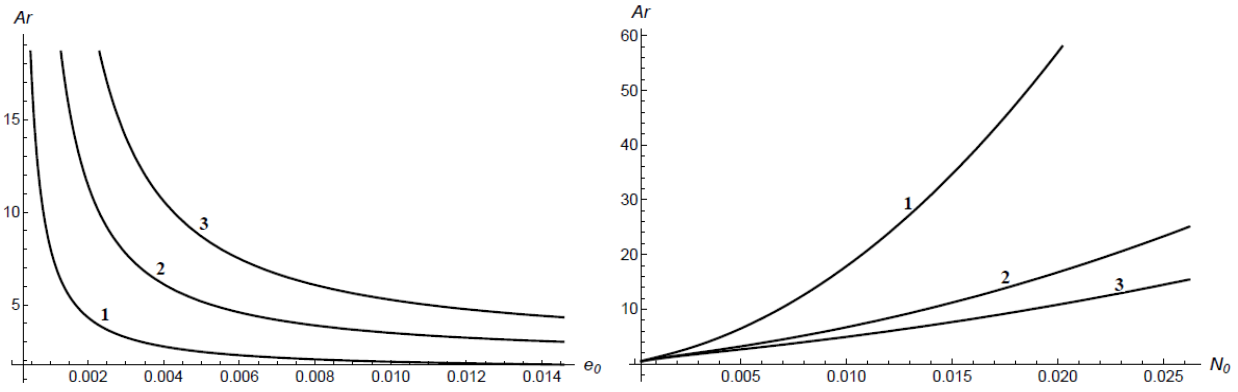

a) b)

Fig.2. Cross-sectional area *Ar* of the right half of FFGL in Fig.1a (curvilinear triangle *ABCA*) as a function of evaporation rate e_0 from the discharge zone at the density contrast γ=0.03 and infiltration rates N_0=0.1, 0.2, 0.3 (curves 1-3, correspondingly) (a); $Ar(N_0)$ at γ=0.03 and e_0=0.1, 0.3, 0.5 (curves 1-3, correspondingly) (b).

Fig.2a and Fig.2b show (respectively) the graphs $Ar(e_0)$ at γ=0.03 and N_0=0.1, 0.2, 0.3 (curves 1-3, correspondingly) and $Ar(N_0)$ at γ=0.03 and e_0=0.1,0.3, 0.5 (curves 1-3, correspondingly).

PK-77 (pp.485-486) pointed out that evaporation from the phreatic surface may not be constant (as assumed above) but rather depends on the depth of this surface counted from the local ground surface. For simplicity, we ignore the relief of the topography above the evapotranspiring arc of FFGL and assume that M_sC_s in Fig.1a is a horizontal line (dashed-dotted) located at an effective depth D_e^* above the undisturbed saline water table. Then the evapotranspiration intensity depends on $d[F_f(x)]$. PK-77 provided field data for $e^*[d^*]$ as a linear function i.e. $e^* = e_0^* - \beta D_e^* + \beta F_f$ where β is a given constant. Then in dimensionless quantities eqn. (3) transforms to

$$\frac{\mathrm{d}^2\Phi_f}{\mathrm{d}x^2}=\begin{cases}-N(\mathrm{x}), \text{ at} & 0\le x\le 1,\\ e_1+e_2\sqrt{\Phi_f(x)}, \quad \text{at} & 1\le x\le L_C,\end{cases} \tag{6}$$

where the constants e_1 and e_2 are directly expressed via e_0, β and D_e. The boundary conditions in BVP (6) are the same as in BVP (3).

The first (linear) equation in (6) integrates into the same elliptical arc as the first eqn.(4) (branch *MC*). The second ODE in (6) is nonlinear with respect to Strack's potential but it integrates in elliptic functions. For the sake of brevity we skip over computations of g_f and g_s obtained as solutions of BVP (6).

3.2 Axisymmetric lenses

If the dune surface B_sC_s (Fig.1a) resembles a cupola (barchan dunes, see e.g. Bishop, 2013) and infiltration originates from a disk-shaped spot of rainfall at the crest of this cupola (co-axial with the cupola), then flow in FFGL is axisymmetric. The saturated water storage is equal to the volume V_f^* of the corresponding body of revolution. Kunin reported axisymmetric shapes of MAR-fed FFGLs (see the field data on the Sansyz lens from Kunin, 1959, supplementary file 4).

The DF model for axisymmetric flows reduces to the following nonlinear ODE:

$$\frac{1}{R}\frac{\mathrm{d}}{\mathrm{d}R}\left(Rk\ (\mathrm{F}_f+F_s)\frac{\mathrm{d}F_f}{\mathrm{d}R}\right)=\begin{cases}-N^*(R), \text{ at} & 0\le R\le R_M^*,\\ e^*(R), \quad \text{at} & R_M^*\le R\le R_C^*.\end{cases} \tag{7}$$

We introduce dimensionless quantities:

$$(g_s, g_f, \mathrm{r}, y, b, m, r_C)=(F_s, F_f, R, Y, b^*, m^*, R_C^*)/R^*_M,\ V_f=V_f^*/R_M^{*2}.$$

Eqn.(7) reads:

$$\frac{\mathrm{d}}{\mathrm{d}}\left[r\frac{\mathrm{d}g_f}{\mathrm{d}r}\right]=\begin{cases}-N(r)r, \text{ at} & 0\le r\le 1,\\ e(r)r, \quad \text{at} & 1\le r\le r_C.\end{cases} \tag{8}$$

If the infiltration and evaporation rates are constant (N_0 and e_0), then - similarly to the case of a linear dune - eqn.(8), with the same boundary conditions as in the previous Section, integrates this BVP to:

$$g_f = \begin{cases} \sqrt{(e_0 + N_0)\,\mathrm{Log}(1 + N_0 / e_0) - N_0 r^2}\ / \sqrt{2}, \ \text{at } 0 \le r \le 1, \\ \sqrt{(N_0 + e_0)\,\mathrm{Log}[r\sqrt{1 + N_0 / e_0}] + e_0 r^2 - (N_0 + e_0)}\ / \sqrt{2}, \quad \text{at } 1 \le r \le r_C = \sqrt{1 + N_0 / e_0}. \end{cases} \tag{9}$$

A dimensionless volume of FFGL is

$$V_f = 2\pi(1 + 1/\gamma) \int_0^{\sqrt{1+N_0/e_0}} r\, g_f(\mathrm{r})\, \mathrm{d}r \,. \tag{10}$$

We put eqn.(9) as an integrand in eqn.(10) and computed V_f with the routines of Wolfram's (1991) *Mathematica*.

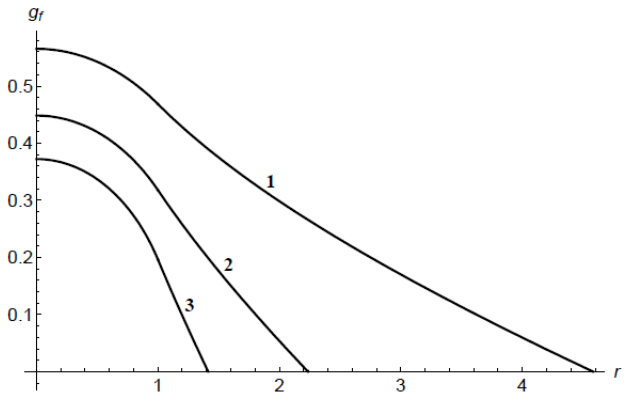

Fig.3a

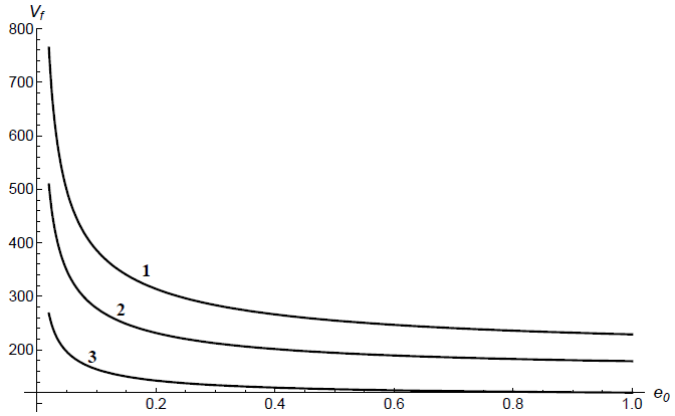

Fig.3b

Fig. 3. The water table $g_f(r)$ axisymmetric FFGL for N_0 =0.2 , γ =0.03 and e_0=0.01, 0.05, 0.2 (curves 1-3, correspondingly) (a). Saturated water storage in FFGL $V_f(e_0)$ for γ =0.03 and N_0=0.1, 0.2, 0.3 (curves 1-3) (b).

Fig.3a shows the water table of axisymmetric FFGL for N_0 =0.2 , γ =0.03 and e_0=0.01, 0.05, 0.2 (curves 1-3, correspondingly). Apparently, the evaporating branch of the phreatic surface is almost straight, especially, close to the point $r=r_C$ where the fresh water zone tapers to the saline phreatic horizon. Fig 3b shows $V_f(e_0)$ for γ =0.03 and N_0=0.1, 0.2, 0.3 (curves 1-3). Here – similarly to Fig.2b – we see that the saturated storage of FFGL is most sensitive to the intensity of evaporation at small e_0.

4. Two-Dimensional Flow in a Linear Dune

Now we consider 2-D flow in in a vertical plane of FFGL under a linear dune. Similarly to groundwater systems modeled by PK-77, Strack, 1978 and Van Der Veer, 1977, a rigorously stated mathematical problem involves three free boundaries, *viz*. a branch of the phreatic surface with accretion, a branch with evaporation and interface. Then, the corresponding domain in the hodograph plane is a curvilinear quadrangle. For such polygons, an analytical solution by the PK-77 method becomes prohibitively complicated[2]. In this Section, we circumvent conformal mappings of a curvilinear polygon in the hodograph plane (see PK-77, her Fig. 224 and 227) by approximating the free boundaries by straight segments.

The interface CA can be approximated reasonably by a straight line. In the DF model the interface under infiltrated phreatic surface usually has a high degree of curvature close to point A (see the elliptical phreatic surfaces and interfaces found in PK77 and van der Veer (1977) in terms of 2-D potential and DF models for an island lens). Similarly, the DF model predicts an elliptic phreatic surface in Fig.3 of Haitjema and Mitchell-Bruker (2005) in case of uniform infiltration and equal levels of water in the reservoirs. However, in case of a uniform evaporation the phreatic surface in Fig.3 of Haitjema and Mitchell-Bruker (2005) at small evaporation rates becomes a hyperbola. At high evaporation the hyperbola splits into two

[2] We recall that PK-77 effectively solved simpler 2-D problems with either constant recharge or constant evaporation intensity along the whole water table, see her Figs. 223 and 225, with a curvilinear triangle in the hodogrpah plane (see also Maas, 2007). Strack (1978) solved the problem with a variable infiltration-evaporation but in an unconfined aquifer without a subjacent bedrock.

straight lines bounding two hydraulically disconnected saturated wedges (see e.g. Kacimov et al., 2003, Youngs, 1974). Similarly, for the case of an interface rather than a horizontal bedrock of Haitjema and Mitchell-Bruker (2005) at point *A* of our Fig.1a a wedge depicted in Fig.8 of van der Veer (1978) emerges. Kunin's (1959) field observation (see the supplementary file 2) illustrate that both phreatic surface and interface flatten towards point A in our Fig.1a. Therefore, the slope of *BMC* is zero at point *B*, relatively high at point *M* and small again at point *A*. This is also illustrated by the behavior of curves 1-3 in Fig.3. Our straight-line BMA and Ghijben-Herzberg *CA* are, hence, a reasonable approximation of a real phreatic surface and interface, which have inflection points. From field observations-records of the water table of numerous FFGLs (Kunin, 1959), one can easily get the loci of points *B* and *C* in the physical plane i.e. b^* and L^* in Fig.1a. Next, we assume that the Ghijben-Herzberg relation holds at point *A*, i.e. $Y_A = -b^*/\gamma$. We also approximate the curved phreatic surface and interface (solid lines in Fig.4a) by straight segments *BC* and *BA* (dashed lines), i.e. we get a triangle *BAC* (G_z which is a Tothian unit basin of this problem) as the right half of FFGL. We solve a 2-D problem in G_z.

4.1.*Toth's model with a fixed straight phreatic surface and interface as free surface*

As usually, we introduce a complex physical coordinate $z = x + \mathrm{i}\, y$, velocity potential $\phi^* = -kh_f$ of the moving fresh water where $h_f(x, y)$ is the hydraulic head in the fresh water counted from point *C*. The complex potential $w^* = \phi^* + \mathrm{i}\psi^*$, where ψ^* is a stream function. Point *C* in Fig.4a is selected as fiducial and the complex potential domain G_{w*} corresponding to G_z is shown in Fig.4b. The curve *BMC* of the digone G_{w*} is not known. The specific discharge vector is $\vec{V} = \nabla\phi^*$. The pressure head and pressure in fresh water are $p_f(x, y) = -(\phi^*/k + y)$ and $P_f = \rho_f g p_f$, correspondingly. The pressure head and pressure in saline water are $p_s(y) = -y$, and $P_s = \rho_s g p_s$, correspondingly.

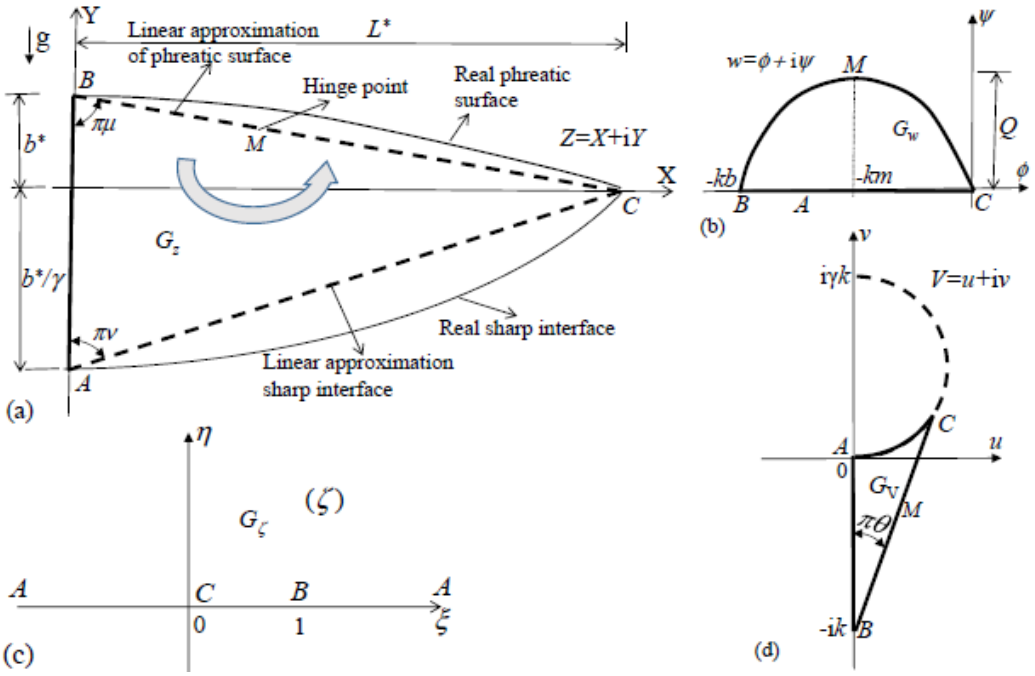

Fig.4. Saturated triangle G_z (half of FFGL) in vertical cross-section of the Toth-type flow (a), digon G_w in the complex potential domain corresponding to G_z (b), reference plane G_ζ (c), curvilinear triangle G_V in the hodograph plane for BVP in the Appendix (d).

Thus, the BVP is:

$$\begin{cases} \Phi^* + k_s y = 0, & \text{along } BC, \\ \Psi^* = 0, & \text{along } AC, \\ \Phi^* = 0, & \text{along } AB. \end{cases} \tag{11}$$

We recall that in the 1960-s Toth (2009) solved a similar BVP in a rectangle (by the method of separation of variables in the Laplace equation); Kacimov (1996) and Al-shukeili et al. (2019) solved a mixed BVP in a trapezium and pentagon, correspondingly. Unlike the DF approximation of Section 2, the widths of the infiltration and exfiltration segments in Fig.4a are not specified but are found as a part of solution i.e. the locus of point *M* is determined. Moreover, by assuming isobaric condition along a given line (*BC* in our case) the Toth model automatically requires determination of the intensities of inflow through *BM* and exfiltration through *MC*, which were also input parameters of the DF model.

We use the Schwarz-Christoffel formula and map conformally the triangle G_z onto the half plane G_ζ in Fig.4c with the correspondence of points $(C, B, A) \to (0,1,\infty)$

$$\mathrm{Z}(\varsigma) = \mathrm{i}\mathrm{e}^{\mathrm{i}\pi\mu}\mathrm{c}\int_0^{\varsigma} t^{-\mu-\nu}(1-t)^{\mu-1}\mathrm{d}t + L_C^* = \mathrm{i}\mathrm{e}^{\mathrm{i}\pi\mu}\mathrm{c}\,\mathrm{B}_{\varsigma}(1-\mu-\nu,\mu) + L_C^*, \tag{12}$$

where B_{ς} is the incomplete Beta-function and a real constant c is determined from the condition $\mathrm{Im}\, Z(1) = b^*$ as

$$c = b^* / \left(\cos\pi\mu\,\mathrm{B}(1-\mu-\nu,\mu)\right), \tag{13}$$

The angles of G_z are $\tan[\pi\mu] = L^* / \mathrm{b}^*$, $\tan[\pi\nu] = \gamma L^* / \mathrm{b}^*$, and $\mathrm{B}(\mu,\nu)$ is the complete Beta-function.

From eqn.(10) along *BC*

$$Y(\xi) = b^* \frac{\mathrm{B}_{\xi}(1-\mu-\nu,\mu)}{\mathrm{B}(1-\mu-\nu,\mu)}, \quad 0 < \xi < 1, \tag{14}$$

where $\mathrm{B}_{\xi}(1-\mu-\nu,\mu)$ is the incomplete Beta-function.

From eqn.(11) the analytic functions $w^*(\varsigma)/\sqrt{\varsigma(1-\varsigma)}$ obeys a nonhomogeneous Dirichlet's boundary condition

$$\mathrm{Re}\left[\, w^*(\xi)/\sqrt{\xi(1-\xi)}\,\right] = -kY(\xi)/\sqrt{\xi(1-\xi)} \text{ at } \xi \in (0,1),$$

$$\mathrm{Re}\left[\, w^*(\xi)/\sqrt{\xi(1-\xi)}\,\right] = 0 \text{ at } \xi \in (-\infty,0)\cup(1,\infty).$$

The function $w^*(\varsigma)/\sqrt{\varsigma(1-\varsigma)}$ vanishes at infinity and has integrable singularities at the points $\varsigma = 0$ and $\varsigma = 1$. Therefore (see Henrici, 1993) the last Dirichlet problem is uniquely solvable and its solution gives the Schwarz operator for a half-plane. Thus, we obtain

$$w^*(\varsigma)=\frac{kb^*\sqrt{\varsigma(1-\varsigma)}}{\pi \mathrm{i}\,\mathrm{B}(1-\mu-\nu,\mu)}\int_0^1\frac{\mathrm{B}_t(1-\mu-\nu,\mu)\mathrm{d}t}{\sqrt{t(1-t)}(t-\varsigma)}\ . \tag{15}$$

From eqns. (14), (15), along the isobar *BC* we apply the Plemelj-Sokhotski formula (see Henrici, 1993):

$$\psi^*(\xi)=\frac{kb^*\sqrt{\xi(1-\xi)}}{\pi\,\mathrm{B}(1-\mu-\nu,\mu)}\int_0^1\frac{\mathrm{B}_t(1-\mu-\nu,\mu)\mathrm{d}t}{\sqrt{t(1-t)}(t-\xi)},\quad 0<\xi<1. \tag{16}$$

The integral in eqn. (16) is singular and is understood in the sense of principal value (Henrici, 1993). The stream function attains its unique and global maximum at a hinge point *M* (see Fig.4b) that quantifies the total flow rate, *Q*, of fresh groundwater flow through FFGL:

$$Q^*=\psi^*(\xi_M).$$

We introduce dimensionless quantities:

$$(x,y,m,L_C,L_M)=(X,Y,m^*,L_C^*,L_M^*)/b^*,\quad (\phi,\psi,Q)=(\phi^*,\psi^*,Q^*)/(kb^*)$$

For computations of the integrals in eqn.(16) we used the **NIntegrate** function of Wolfram's (1991) *Mathematica*, with the option **PrincipalValue->True** for singular integrals. The flow rate *Q* was computed by applying the *Mathematica* built-in function **FindMaximum** to eqn. (16).

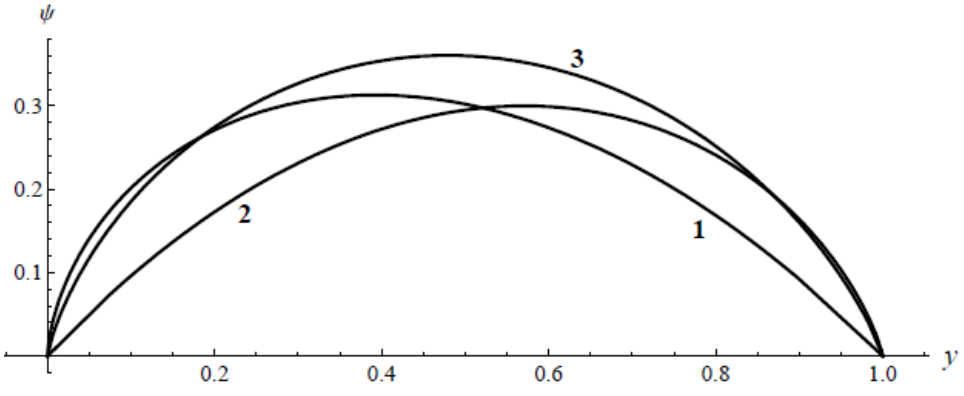

Fig.5. Distribution of the streamfunction in 2-D flow of Fig.4a as a function of the vertical coordinate for three half-width of FFGL, L_C=1, 4.3, 30 (curves 1-3) at γ=0.03.

Fig.5 plots the distribution $\psi(y)$ along *BC* for L_C=1, 4.3, 30 (curves 1-3) at γ=0.03. These curves show that with steepening of the phreatic surface the maximum of ψ (attained at the hinge point *M*) shifts towards point *B*. We also varied continuously L_C and found the maximum of the function $Q(L_C)$ at γ=0.03.This maxi-max is attained at $L_C \approx 4.3$ and is $Q_{\max} \approx 0.36$. The elevation of point *M* is $y_M \approx 0.48$. This simple optimization can be used for *apriori* estimations of *Q*, *viz.* for a measured peak b^* of the water table we can immediately write the bound $Q<Q_{max}$, whatever is the FFGL width $2L_C$. This width, unlike the height *b* of the groundwater mound (commonly located somewhere in the middle of the MAR pond) is not easy to precisely measure (see the vertical profile of the Sansyz FFGL, Kunin, 1959, supplementary file 2).

5. Suggestions for future work

Our analytical solutions allow to carry out the analysis of vulnerability of recharge-evaporation controlled FFGLs to variation of the basic input parameters: intensities of the distributed sink-source along phreatic surfaces, similarly to what has been done for other TFLs (Laattoe et al. , 2017) and for lenses in oceanic islands and coastal dunes (Morgan and Werner, 2014, Stuyfzand and van der Schans, 2018). Exploitation of desert FFGLs, especially, ones only naturally recharged, requires smart skimming of the fresh water because overabstraction causes a rapid brackization (Kunin,1959). A potential can be used for modeling of horizontal or vertical wells tapping FFGLs (Hocking and Forbes, 2004). As in Morgan and Werner (2014), Stuyfzand and van der Schans (2018), our analytical models assume steady flows, although a real focused post-rain infiltration to *BM* in Fig.1a comes in short pulses. The real dunes are not homogeneous and isotropic media as we assumed but are structured (Lancaster, 1995) that complicates the infiltration-evaporation paths of pore water and determination of the interface-

phreatic surface inside the dune bodies (Al-Shukaili et al., 2019, Bagnold, 2012, Berndtsson and Chert, 1994, Berndtsson et al.,1996, Dose et al., 2014, McCord et al., 1991, McCord and Stephens, 1987, Pye and Tsoar, 2008, Chapter 7). Also, dispersion blurs the interface of FFGL. Further laboratory (e.g. sandbox) and numerical modeling , as well as field piezometry, measurements of TDS and matrix potential in desert FFGLs should be done, similarly to analogous SWI problems (see e.g. Houben et al., 2018).

6. Concluding Remarks

Kunin's FFGLs are unique hydrological entities which emerge in desert climates with a spatially focused natural recharge to a part of the water table from a dune crest or with a MAR infiltration from a surface pond. An intensive evaporation from the tail (not recharged part) of the water table supports an FFGL-scale water motion in sand. In order to float these lenses require a substrate of saline groundwater (an unconfined aquifer) of a sufficient depth and small natural hydraulic gradient. In these conditions, FFGL is subtended by a trough-shaped interface between a moving fresh water inside the lens and static saline water. This interface has the same confining role as the bedrock in the Toth (2009) regional flow but unlike the fixed lower boundary of the Toth unit basin (determined by geological stratification) the interface supporting FFGL is a free boundary, i.e. not fixed but depending on hydraulic conductivity of the sand, recharge and evaporation intensities, the width of the infiltration spot and densities of fresh and saline groundwater. FFGL resembles a fresh-water MAR "bubble" completely submerged into saline groundwater (Kacimov et al. 2018). Analytical solutions to BVPs for steady state regimes described by ODEs (DF model) for Strack's potential give the shapes of the water table and interface (including the locus of the crest and total width of FFGL). Remarkably, an evaporating segment of the FFGL and therefore the DF interface are straight lines, provided the recharge-evaporation intensities are constant, as was the case in the Van Der Veer (1977) solution to an SWI problem. For 2-D flows in FFGL, holomorphic characteristic functions are used with the help of Toth's approximation of the upper boundary of the flow domain as a fixed isobar in

gravity-driven groundwater flows. Half of the flow domain is considered as a Tothian unit basin. This triangle or curvilinear triangle is made of an isobar and streamline.

Acknowledgments.

This work was supported by SQU, grant IG/CAMS/SWAE/18/01, and by the subsidy allocated to Kazan Federal University for the state assignment in the sphere of scientific activities, project № 1.12878.2018/12.1. Helpful comments by O.D.L. Strack and an anonymous referee are appreciated.

Appendix

Toth's model with a fixed straight phreatic surface and interface as a free surface

In this Appendix, we extend the Toth model of Subsection 4.1 by assuming that the interface, *AC*, is not a straight segment but a free boundary. The upper boundary of the lens, *BMC*, as in Subsection 4.1, is still not a free boundary but a given straight tilted isobaric segment of a slope *s* and elevation *b* above the background saline water table. Even with this simplification, to get an analytical solution we engage the machinery of integral representations of the Riemann-Hilbert BVP (Henrici, 1993, PK-77). This BVP is formulated as following:

$$\begin{cases} \psi = 0, \quad \phi - k\gamma y = 0 \text{ along } AC, \\ y = b - s\,x, \quad \phi + ky = 0 \quad \text{along } BMC, \\ \psi = 0, \quad x = 0 \text{ along } BA, \end{cases} \tag{A1}$$

where b and L_c are given constants,

$$\gamma = \rho_s / \rho_f - 1, \; s = b / L_c = \tan\theta . \tag{A2}$$

From (A1) the hodograph, G_V, is a circular triangle shown in Fig.4d (see PK-77 for details of hodographs in interface flows, in particular her Fig.227). First, we map conformally the circular triangle symmetric to G_V with respect to the real axis in Fig.4d onto the same

reference half-plane G_ς in Fig.4c. The correspondence of points is $(C,B,A)\to(0,1,\infty)$. The mapping function is (Koppenfels and Stallman,1959) is:

$$\omega(\varsigma)=\mathrm{i}k-\mathrm{i}kc\left(\frac{\varsigma-1}{\varsigma}\right)^{\theta}\frac{\mathrm{F}(1/4+\theta/2-\lambda/2,1/4+\theta/2+\lambda/2;1+\theta;1-1/\varsigma)}{\mathrm{F}(1/4-\theta/2-\lambda/2,1/4-\theta/2+\lambda/2;1-\theta;1-1/\varsigma)}, \tag{A3}$$

where F stands for a hypergeometric function ${}_2\mathrm{F}_1$, $0<\arg(1-1/\varsigma)<\pi$,

$$c=\frac{\Gamma(3/4+\theta/2+\lambda/2)\Gamma(3/4+\theta/2-\lambda/2)\Gamma(1-\theta)}{\Gamma(3/4-\theta/2+\lambda/2)\Gamma(3/4-\theta/2-\lambda/2)\Gamma(1+\theta)},\qquad \pi\lambda=\arccos\left[\frac{2+\gamma}{\gamma}\sin\pi\theta\right]. \tag{A4}$$

Here $\pi\lambda$ is the angle at the vertex *C* of the triangle G_V. From (A4) and (A2) follows that γ must satisfy the inequality $\gamma\le 2s/(\sqrt{s^2+1}+s)$.

Remark. The hypergeometric functions in (A3) are defined for $\varsigma\in(1/2,\infty)$. If $\varsigma\in(-\infty,1/2)$ then we have to use the analytic continuation (Abramowitz and Stegun, 1969, formula 15.3.7), which gives

$$\omega(\varsigma)-\mathrm{i}k=-\mathrm{i}ke^{\mathrm{i}\pi\theta}\frac{f(\varsigma;\theta,\lambda)+f(\varsigma;\theta,-\lambda)}{f(\varsigma;-\theta,\lambda)+f(\varsigma;-\theta,-\lambda)}, \tag{A5}$$

where

$$f(\varsigma;\theta,\lambda)=e^{-\mathrm{i}\pi\lambda/2}\left(\frac{\varsigma-1}{\varsigma}\right)^{\lambda/2}\frac{\Gamma(\lambda)\Gamma\left(\frac{3}{4}+\frac{\theta-\lambda}{2}\right)\mathrm{F}\left(\frac{1}{4}+\frac{\theta-\lambda}{2},\frac{1}{4}-\frac{\theta+\lambda}{2};1-\lambda;\frac{\varsigma}{\varsigma-1}\right)}{\Gamma(1/4+(\theta+\lambda)/2)}. \tag{A6}$$

Next, we introduce two functions $F(\varsigma)=\mathrm{d}w/\mathrm{d}\varsigma$ and $Z(\varsigma)=\mathrm{d}z/\mathrm{d}\varsigma$, and reformulate the boundary conditions (A1) in G_ς as the two-dimensional Riemann BVP (Gakhov, 1966)

$$\begin{aligned}
&\mathrm{Im}\left[\mathrm{i}\,F(\xi)-k\gamma Z(\xi)\right]=0,\quad \mathrm{Im}\,F(\xi)=0, && -\infty<\xi<0;\\
&\mathrm{Im}\left[\mathrm{i}F(\xi)+kZ(\xi)\right]=0,\quad \mathrm{Im}\left[e^{\mathrm{i}\pi\theta}\,Z(\xi)\right]=0, && 0<\xi<1;\\
&\mathrm{Im}\left[\mathrm{i}\,Z(\xi)\right]=0,\quad \mathrm{Im}\,F(\xi)=0, && 1<\xi<\infty.
\end{aligned} \tag{A7}$$

Now, using the relation $F(\varsigma)=\omega(\varsigma)Z(\varsigma)$, from eqn. (A7) we can obtain two equivalent scalar Riemann BVPs with respect to $F(\varsigma)$ or $Z(\varsigma)$. The latter BVP takes the form

$$\begin{aligned} &\mathrm{Im}\left[\omega(\varsigma)Z(\xi)\right]=0, \quad -\infty<\xi<0;\\ &\mathrm{Im}\left[e^{\mathrm{i}\pi\theta}\,Z(\xi)\right]=0, \qquad 0<\xi<1;\\ &\mathrm{Im}\left[\mathrm{i}\,Z(\xi)\right]=0, \qquad 1<\xi<\infty. \end{aligned} \tag{A8}$$

We introduce a new function $Z_1(\varsigma)$ by

$$Z(\varsigma)=e^{-\mathrm{i}\pi\theta}(1-\varsigma)^{1/2-\theta}Z_1(\varsigma), \tag{A9}$$

where the branch of the function $(1-\varsigma)^{1/2-\theta}$ is fixed in the upper half-plane to be positive at $0<\xi<1$. The function (A9) transforms BVP (A8) to the following homogeneous Riemann BVP:

$$\begin{aligned} &\mathrm{Im}\left[e^{-\mathrm{i}\pi\theta}\omega(\varsigma)Z_1(\xi)\right]=0, \quad -\infty<\xi<0;\\ &\mathrm{Im}\left[Z_1(\xi)\right]=0, \quad 0<\xi<\infty. \end{aligned} \tag{A10}$$

Solution to problem (A10) is sought in the class of functions with an integrable singularity at the point $\varsigma=0$ and a zero at infinity, the order of this zero is more than one. From the second condition (A10) and the representation (A9) follows that $\varsigma=1$ is a simple pole of $Z_1(\varsigma)$.

Next, we introduce the function

$$\chi(\varsigma)=\exp\left[\frac{1-\varsigma}{2\pi\mathrm{i}}\int_{-\infty}^{0}\log\left(e^{\mathrm{i}2\pi\theta}\frac{\overline{\omega(t)}}{\omega(t)}\right)\frac{\mathrm{d}t}{(t-1)(t-\varsigma)}\right]=\varsigma^{-\theta}\exp\left[\frac{\varsigma-1}{\pi}\int_{-\infty}^{0}\frac{\arg\omega(t)\mathrm{d}t}{(t-1)(t-\varsigma)}\right]. \tag{A11}$$

This function vanishes at infinity. If ς approaches the real axis at $\xi\in(-\infty,0)$ from the upper half-plane, then the limit value of $\chi(\varsigma)$, obtained via the Plemely-Sokhotski formula (Henrici, 1993), follows from eqn.(A11) as:

$$\chi(\xi)=e^{-\mathrm{i}\pi\theta}(-\xi)^{-\theta}\sqrt{\frac{\omega(\xi)}{\overline{\omega(\xi)}}}\exp\left[\frac{\xi-1}{\pi}\int_{-\infty}^{0}\frac{\arg\omega(t)\mathrm{d}t}{(t-1)(t-\xi)}\right]. \tag{A12}$$

At the vicinity of zero we have

$$\exp\left[\frac{\varsigma-1}{\pi}\int_{-\infty}^{0}\frac{\arg\omega(t)\mathrm{d}t}{(t-1)(t-\varsigma)}\right]=\varsigma^{-1/4+(\theta+\lambda)/2}\chi_0(\varsigma), \tag{A13}$$

where $-1/4+(\theta+\lambda)/2=\arg\omega(0)/\pi$ and the function $\chi_0(\varsigma)$ is continuous and not vanishing at the point $\varsigma=0$.

579 Taking into account eqns.(A11), (A12), (A13) and the boundary condition $\mathrm{Im}\,\chi(\xi)=0$ for

580 $\xi\in(0,\infty)$, we infer that the function

581 $$Z_2(\varsigma)=Z_1(\varsigma)\chi(\varsigma) \tag{A14}$$

582 satisfies a homogeneous boundary condition $\mathrm{Im}\,Z_2(\xi)=0$ at $\xi\in(-\infty,\infty)$.

583 Clearly, $Z_2(\varsigma)$ has simple poles at the points $\varsigma=0$, $\varsigma=1$, and zero of the second order at

584 infinity. Hence

585 $$Z_2(\varsigma)=\frac{c_1}{\varsigma(1-\varsigma)}, \tag{A15}$$

586 where c_1 is an arbitrary real constant to be determined later. Taking into account eqns. (A9),

587 (A11), (A14), and (A15) we obtain the following integral solution to the Dirichlet BVP:

588 $$Z(\varsigma)=c_1e^{-\mathrm{i}\pi\theta}(1-\varsigma)^{-1/2-\theta}\varsigma^{\theta-1}\exp\left[\frac{1-\varsigma}{\pi}\int\limits_{-\infty}^{0}\frac{\arg\omega(t)\mathrm{d}t}{(t-1)(t-\varsigma)}\right],\quad F(\varsigma)=\omega(\varsigma)Z(\varsigma)\ . \tag{A16}$$

589 We integrate $Z(\varsigma)$ in eqn. (A16) and get

590 $$\mathrm{z}(\varsigma)=\int\limits_0^{\varsigma}Z(t)\mathrm{d}t+L_C\,,\quad w(\varsigma)=\int\limits_0^{\varsigma}F(t)\mathrm{d}t\,. \tag{A17}$$

591 The constant c_1 is determined from eqns. (A16), (A17) using the condition $z(1)=\mathrm{i}b$, or

592 $$\mathrm{Im}\int\limits_0^1 Z(t)\mathrm{d}t=-c_1\sin\pi\theta\int\limits_0^1(1-t)^{-1/2-\theta}t^{\theta-1}\exp\left[\frac{1-t}{\pi}\int\limits_{-\infty}^{0}\frac{\arg\omega(\tau)\mathrm{d}\tau}{(\tau-1)(\tau-t)}\right]\mathrm{d}t=b\,.$$

593 Using the last relation, eqns. (A16), (A17) and taking into account that

594 $\omega(\xi)=\mathrm{i}\,k-\mathrm{i}e^{\mathrm{i}\pi\theta}\,|\,\omega(\xi)-\mathrm{i}\,k\,|$ for $\xi\in(0,1)$, we obtain

595 $$\psi(\xi)=b\,\frac{\displaystyle\int\limits_0^{\xi}(|\,\omega(t)-\mathrm{i}\,k\,|-k\cos\pi\theta)(1-t)^{-1/2-\theta}t^{\theta-1}\exp\left[\frac{1-t}{\pi}\int\limits_{-\infty}^{0}\frac{\arg\omega(\tau)\mathrm{d}\tau}{(\tau-1)(\tau-t)}\right]\mathrm{d}t}{\displaystyle\sin\pi\theta\int\limits_0^1(1-t)^{-1/2-\theta}t^{\theta-1}\exp\left[\frac{1-t}{\pi}\int\limits_{-\infty}^{0}\frac{\arg\omega(\tau)\mathrm{d}\tau}{(\tau-1)(\tau-t)}\right]\mathrm{d}t}\,. \tag{A18}$$

It is clear that the function (A18) achieves its maximum at the point $\xi_0 \in (0,1)$ such that

$$| \omega(\xi_0) - \mathrm{i}\, k | = k \cos \pi\theta \,. \qquad \text{(A19)}$$

This completes solution of BVP (A1).

References

+Abramowitz, M. and Stegun, I.A. 1969. Handbook of Mathematical Functions. Dover, New York.

+Al-Weshah, R.A. and Yihdego, Y., 2016. Flow modelling of strategically vital freshwater aquifers in Kuwait. Environmental Earth Sciences, 75(19), 1315.

+Al-Shukaili, A. Al-Busaidi, H., Al-Maktoumi, A., Abdalla, O., Shelukhina, O., and Kacimov, A.R. , 2019. Oblique porous composite as evaporating "cap": Do desert dunes preserve moisture by capillary barriers and tilt of their slopes? Water Resources Research (in press) doi: 10.1029/2018WR024526.

+Babaev A.G. (ed.), 1999. Desert Problems and Desertification in Central Asia: The Researches of the Desert Institute, Springer, Berlin.

+Bagnold, R.A., 2012. The Physics of Blown Sand and Desert Dunes. Courier Corporation.

+Bairamova, I.A., 2013. Of ground fresh water of the Karakum desert Yazkhan lens. Problems of Desert Development, N3-4, 24-27 (in Russian).

+Bakker, M., 2000. The size of the freshwater zone below an elongated island with infiltration. Water Resources Research, 36(1), 109-117.

+Berndtsson, R. and Chert, H., 1994. Variability of soil water content along a transect in a desert area. J. Arid Environment, 27, 127-139.

+Berndtsson, R., Nodomi, K., Yasuda, H., Persson, T., Chen, H. and Jinno, K., 1996. Soil water and temperature patterns in an arid desert dune sand. J. Hydrology, 185(1-4), 221-240.

+Bishop, M.A., 2013. Dune field development, interactions and boundary conditions for crescentic and stellate megadunes of the Al Liwa Basin, the Empty Quarter. Earth Surface Processes and Landforms, 38(2), 183-191.

+Cendón, D.I., Larsen, J.R., Jones, B.G., Nanson, G.C., Rickleman, D., Hankin, S.I., Pueyo, J.J. and Maroulis, J., 2010. Freshwater recharge into a shallow saline groundwater system, Cooper Creek floodplain, Queensland, Australia. J. Hydrology, 392(3-4), 150-163.

+Chamizo, S., Belnap, J., Eldridge, D.J., Cantón, Y. and Issa, O.M., 2016. The role of biocrusts in arid land hydrology. In "Biological Soil Crusts: An Organizing Principle in Drylands", 321-346. Springer.

+Chesnaux, R. and Allen, D.M., 2008. Groundwater travel times for unconfined island aquifers bounded by freshwater or seawater. Hydrogeology J., 16(3), 437-445.

+Danin, A., 2012. Plants of Desert Dunes. Springer.

+Dedkov, V.P., 2011. On the cause of vanishing black saksaul trees in Eastern Karakums and consequences of this phenomenon for ecology and economy of the desert. Proc. Immanuel Kant Baltic Federal University, Ser. Of Natural and Medical Sciences (in Russian).

+Dose, E.J., Stoeckl, L., Houben, G.J., Vacher, H.L., Vassolo, S., Dietrich, J. and Himmelsbach, T., 2014. Experiments and modeling of freshwater lenses in layered aquifers: steady state interface geometry. J. Hydrology, 509, 621-630.

+Eeman, S., Leijnse, A., Raats, P.A.C. and Van der Zee, S.E.A.T.M., 2011. Analysis of the thickness of a fresh water lens and of the transition zone between this lens and upwelling saline water. Advances in Water Resources, 34(2), 291-302.

+Eeman, S., 2017. Dynamics of rainwater lenses on upward seeping saline groundwater. PhD dissertation, Wageningen University.

+Fleskens, L., Ataev, A., Mamedov, B. and Spaan, W.P., 2007. Desert water harvesting from takyr surfaces: assessing the potential of traditional and experimental technologies in the Karakum. Land Degradation & Development, 18(1), 17-39.

+Gael, A.G. and Smirnova, L.F., 1999. Sands and Sandy Soils. GEOS, Moscow (in Russian).

+Gakhov, F.D., 1966. Boundary Value Problems. Addison Wesley, New York.

+Haitjema, H.M. and Mitchell-Bruker, S., 2005. Are water tables a subdued replica of the topography? Groundwater, 43(6), 781-786.

+Hampton, E.R., 1963. Ground water in the coastal dune area near Florence, Oregon. Geological Survey Water-Supply Paper 1539-K, US Department of Interior, Washington, DC.

+Henrici, P., 1993. Applied and Computational Complex Analysis. Volume 3: Discrete Fourier Analysis, Cauchy Integrals, Construction of Conformal Maps, Univalent Functions. Wiley. New York.

+Hocking, G.C. and Forbes, L.K., 2004. The lens of freshwater in a tropical island—2d withdrawal. Computers & Fluids, 33(1), 19-30.

+Houben, G.J., Koeniger, P. and Sültenfuß, J., 2014a. Freshwater lenses as archive of climate, groundwater recharge, and hydrochemical evolution: Insights from depth-specific water isotope analysis and age determination on the island of Langeoog, Germany. Water Resources Research, 50(10), 8227-8239.

+Houben, G., Noell, U., Vassolo, S., Grissemann, C., Geyh, M., Stadler, S., Dose, E.J. and Vera, S., 2014b. The freshwater lens of Benjamín Aceval, Chaco, Paraguay: a terrestrial analogue of an oceanic island lens. Hydrogeology J., 22(8), 1935-1952.

+Houben, G.J., Stoeckl, L., Mariner, K.E. and Choudhury, A.S., 2018. The influence of heterogeneity on coastal groundwater flow-physical and numerical modeling of fringing reefs, dykes and structured conductivity fields. Advances in Water Resources, 113, 155-166.

+Hydrogeology of the USSR. Turkmenskaya SSR. 1972. XXXVIII. Moscow, Nedra (in Russian).

+Kacimov, A.R., 1996. Explicit solutions for seepage infiltrating into a porous earth dam due to precipitation. International J. for Numerical and Analytical Methods in Geomechanics, 20, 715-723.

+Kacimov, A.R., and Obnosov, Yu.V. 2015. An exact analytical solution for steady seepage from a perched aquifer to a low-permeable sublayer: Kirkham-Brock's legacy revisited. Water Resources Research, 51, 3093–3107.

+Kacimov, A., Obnosov, Yu.V., and Al-Maktoumi, A. 2018. Dipolic flows relevant to aquifer storage and recovery: Strack's sink solution revisited. Transport in Porous Media, 123(1), 21-44.

+Kacimov A.R., Obnosov Yu.V., and Perret, J., 2004. Phreatic surface flow from a near-reservoir saturated tongue. J. Hydrology , 296, 271-281.

+Kacimov, A.R., Sherif, M.M., Perret, J.S., and Al-Mushikhi, A. 2009. Control of sea-water intrusion by salt-water pumping: Coast of Oman. Hydrogeology J., 17, 541-558.

682 +Kidron, G.J. and Yair, A., 2008. Runoff and erosion processes within a dune system. In
683 Breckle, S.W., Yair, A. and Veste, M. eds. “Arid Dune Ecosystems: the Nizzana Sands in the
684 Negev Desert.”, 239-249. Springer.

685 +Khalaf , F.I., Misak, R. and Al-Dousari, A., 1995. Sedimentological and morphological
686 characteristics of some nabkha deposits in the northern coastal plain of Kuwait, Arabia. J. of
687 Arid Environments, 29(3), 267-292.

688 +Kolodin, M. 1981. Water and Deserts. Moscow, Mysl (in Russian).

689 +Koppenfels, F. and Stallman, S. 1959. Praxis der konformen Abbildung. Springer, Berlin (in
690 German).

691 +Kunin, V.N., 1959. Local Waters in Deserts and Problems in Their Utilization. Moscow, Akad.
692 Nauk SSSR (in Russian).

693 +Kunin, V.N., 1968. The study of local waters in the deserts of the USSR. Soviet Geography,
694 9(6), 469-488.

695 +Kunin, V.N. and Lezhinsky, G.T., 1960. Temporary Surface Runoff and Artificial Formation
696 of Ground Water in the Desert. Academy of Sciences of the USSR, Moscow (in Russian).

697 +Kuznetsov, A.Y., Yakirevich and Sorek, S., 2006. Extraction simulations of fresh groundwater
698 artificial lenses. Proc. 1st SWIM-SWICA Joint Saltwater Intrusion Conference, Cagliari, Italy,
699 September 24-29, 2006, 103-106.

700 +Kwarteng, A.Y., Viswanathan, M.N., Al-Senafy, M.N. and Rashid, T., 2000. Formation of
701 fresh ground-water lenses in northern Kuwait. J. of Arid Environments, 46(2), 137-155.

702 +Lancaster, N., 1995. Geomorphology of Desert Dunes. Routledge, London.

703 +Laattoe, T., Werner, A.D., Woods, J.A. and Cartwright, I., 2017. Terrestrial freshwater lenses:
704 Unexplored subterranean oases. J. Hydrology, 553, 501-507.

+Lopez, O.M., Jadoon, K.Z. and Missimer, T.M., 2015. Method of relating grain size distribution to hydraulic conductivity in dune sands to assist in assessing managed aquifer recharge projects: Wadi Khulays dune field, western Saudi Arabia. Water, 7(11), 6411-6426.

+Maas, C. 2007. Influence of climate change and sea level rise on a Ghijben Herzberg lens. J. Hydrology, 347, 223-228.

+Macumber, P.G., 2003. Lenses, plumes and wedges in the Sultanate of Oman: A challenge for groundwater management. In "Water Resources Perspectives: Evaluation, Management and Policy", pp. 349-370, Ed. by Wood, W.W. and Al-Sharhan, A.S. Elsevier.

+McCord, J.T. and Stephens, D.B., 1987. Lateral moisture flow beneath a sandy hillslope without an apparent impeding layer. Hydrological Processes, 1(3), 225-238.

+McCord, J.T., Stephens, D.B. and Wilson, J.L., 1991. Hysteresis and state-dependent anisotropy in modeling unsaturated hillslope hydrologic processes. Water Resources Research, 27(7), 1501-1518.

+Milewski, A., Sultan, M., Al-Dousari, A. and Yan, E., 2014. Geologic and hydrologic settings for development of freshwater lenses in arid lands. Hydrological Processes, 28(7), 3185-3194.

+Morgan, L.K. and Werner, A.D., 2014. Seawater intrusion vulnerability indicators for freshwater lenses in strip islands. J. Hydrology, 508, 322-327.

+Polubarinova-Kochina, P.Ya., 1977. Theory of Ground Water Movement. Nauka, Moscow (in Russian).

+Pye, K. and Tsoar, H., 2008. Aeolian Sand and Sand Dunes. Springer.

+Rizk, Z.R. and Al-Sharhan, A.S., 2003. Water resources in the United Arab Emirates. In "Water Resources Perspectives: Evaluation, Management and Policy", pp.245-264. Ed. by Wood, W.W. and Al-Sharhan, A.S. Elsevier.

+Rogovskaya, N.V., Vitkovskaya, T.P. and Kravtsov, G.K., 1986. The quantitative aspect of assessment of fresh groundwater resources supplied by infiltration (based on data from the Karrykull Permanent Station). Problems of Desert Development, N2, 69-75.

+Rogovskaya, N.V., Chubarov, V.N. and Semenova-Yerofeyeva, Y.M. 1979. Hydrogeological aspects of mapping aeration zones. International Geology Review, 21(9), 1106-1116.

+Porter P., 2015. The world is not flat: War and distance in the twenty first century. In “Geo-strategy and War: Enduring Lessons for the Australian Army.” Ed. by Denis P., Big Sky Publishing.

+Schevchenko, N.G., 1965. Geomorphological criteria for search lensing fresh waters under conditions of sandy relief. In “Problems of Geology of Turkmenia”, Academy of Sci. Turkmen SSR, Ashkabad. 228-234.

+Schot, P.P., Dekker, S.C. and Poot, A., 2004. The dynamic form of rainwater lenses in drained fens. J. of Hydrology, 293(1-4), 74-84.

+Singh, S.P. and Stammers, W.N., 1989. A potential theory-based finite element algorithm for freshwater recharge of saline aquifers: A sharp interface model. Water Resources Research, 25(7), 1685-1694.

+Strack, O.D.L., 1978. Distributed sources for unconfined groundwater flow in a half-space. J. Hydrology, 39(3-4), 239-253.

+Strack, O.D.L., 1989. Groundwater Mechanics. Prentice Hall, Englewood Cliffs.

+ Stuyfzand, P.J. and van der Schans, M.L., 2018. Effects of intake interruptions on dune infiltration systems in the Netherlands, their quantification and mitigation. Science of The Total Environment, 630, 757-773.

+Tao, L., Honglang, X. and Xinrong, L., 2001. Modeling the effects of crust on rain infiltration in vegetated sand dunes in arid desert. Arid Land Research and Management, 15(1), 41-48.

+Tóth, J., 2009. Gravitational Systems of Groundwater Flow: Theory, Evaluation, Utilization. Cambridge Univ. Press, Cambridge.

+Vacher, H.L., 1988. Dupuit-Ghyben-Herzberg analysis of strip-island lenses. Geological Society of America Bulletin, 100(4), 580-591.

+Van der Veer, P., 1977. Analytical solution for steady interface flow in a coastal aquifer involving a phreatic surface with precipitation. J. Hydrology, 34(1-2), 1-11.

+Van Duijn, C.J. and Schotting, R.J., 2017. The interface between fresh and salt groundwater in horizontal aquifers: The Dupuit–Forchheimer approximation revisited. Transport in Porous Media, 117(3), 481-505.

+Voortman, B.R., 2018. Evaporation From Dry Dune Vegetation. PhD thesis, Vrije Universiteit, Holland.

+Voortman, B.R., Bartholomeus, R.P., Van Der Zee, S.E.A.T.M., Bierkens, M.F.P. and Witte, J.P.M., 2015. Quantifying energy and water fluxes in dry dune ecosystems of the Netherlands. Hydrology and Earth System Sciences, 19(9), 3787-3805.

+Wang, T., Istanbulluoglu, E., Wedin, D. and Hanson, P., 2015. Impacts of devegetation on the temporal evolution of soil saturated hydraulic conductivity in a vegetated sand dune area. Environmental Earth Sciences, 73(11), 7651-7660.

+Werner, A.D. and Laattoe, T., 2016. Terrestrial freshwater lenses in stable riverine settings: Occurrence and controlling factors. Water Resources Research, 52(5), 3654-3662.

+Wolfram, S., 1991. *Mathematica*. A System for Doing Mathematics by Computer. Addison-Wesley, Redwood City.

773 +Yair, A., 2008. Effects of surface runoff and subsurface flow on the spatial variability of water
774 resources in longitudinal dunes. In Breckle, S.W., Yair, A. and Veste, M. eds. "Arid Dune
775 Ecosystems: the Nizzana Sands in the Negev Desert.", 251-269, Springer.

776 +Yair, A., Veste, M. and Breckle, S.W., 2008. Geo-ecology of the north-western Negev sand
777 field. In Breckle, S.W., Yair, A. and Veste, M. eds. "Arid Dune Ecosystems: the Nizzana Sands
778 in the Negev Desert.", 17-24. Springer.

779 +Yakirevich, Q. A., Kuznetsov, M., Sorek, S. and Mamieva, A.I. 2005. Simulating artificial
780 lenses of fresh groundwater in desert conditions. In "Groundwater and Saline Intrusion", Proc.
781 18 Salt Water Intrusion Meeting, Cartagena, 2004, 151-161.

782 +Young, M.E., Macumber, P.G., Watts, M.D., Al-Toqy, N., 2004. Electromagnetic detection of
783 deep freshwater lenses in a hyper-arid limestone terrain. J. of Applied Geophysics, 57, 43–61.

784 Youngs, E.G., 1974. Seepage rates and the horizontal flow approximation. Water Resources
785 Research, 10(4), 874-876.

786 +Zuurbier, K.G., Zaadnoordijk, W.J. and Stuyfzand, P.J., 2014. How multiple partially
787 penetrating wells improve the freshwater recovery of coastal aquifer storage and recovery (ASR)
788 systems: A field and modeling study. J. Hydrology, 509, 430-441.

789

790 **Figure Captions**

791 Fig.1 Vertical cross-section of FFGL recharged from a linear dune (a) and from a takyr (b).

792 Fig.2. Cross-sectional area *Ar* of the right half of FFGL in Fig.1a (curvilinear triangle *ABCA*)
793 as a function of evaporation rate e_0 from the discharge zone at the density contrast γ=0.03 and
794 infiltration rates N_0=0.1,0.2,0.3 (curves 1-3, correspondingly) (a); $Ar(N_0)$ at γ=0.03 and e_0=0.1,
795 0.3, 0.5 (curves 1-3, correspondingly) (b).

796

797 Fig. 3. The water table $g_f(r)$ axisymmetric FFGL for N_0 =0.2 , γ =0.03 and e_0=0.01, 0.05, 0.2
798 (curves 1-3, correspondingly) (a). Saturated water storage in FFGL $V_f(e_0)$ for γ =0.03 and
799 N_0=0.1, 0.2, 0.3 (curves 1-3) (b).

800

801 Fig.4. Saturated triangle G_z (half of FFGL) in vertical cross-section of the Toth-type flow
802 (a), digon G_w in the complex potential domain corresponding to G_z (b), reference plane G_ζ (c),
803 curvilinear triangle G_V in the hodograph plane for BVP in the Appendix (d).

804

805 Fig.5. Distribution of the streamfunction in 2-D flow of Fig.4a as a function of the vertical
806 coordinate for three half-width of FFGL, L_C =1, 4.3, 30 (curves 1-3) at γ=0.03.

807

808

809

810

811 **List of Acronyms**

812 BVP=boundary value problem

813 FFGL=fresh floating groundwater lens

814 MAR=managed aquifer recharge

815 PK-77= Polubarinova-Kochina, P.Ya., 1977. Theory of Ground Water Movement. Nauka,
816 Moscow (in Russian)

817 TFL=terrestrial freshwater lenses